

Slow Relaxation, Spatial Mobility Gradients and Vitrification in Confined Films

Stephen Mirigian^{1,4} and Kenneth S. Schweizer^{1-4,*}

Departments of Materials Science¹, Chemistry², Chemical and Biomolecular

Engineering³ and Frederick Seitz Materials Research Laboratory⁴, University of Illinois,

Urbana, IL 61801

[*kschweiz@illinois.edu](mailto:kschweiz@illinois.edu)

Abstract

Two decades of experimental research indicates that spatial confinement of glass-forming molecular and polymeric liquids results in major changes of their slow dynamics beginning at large confinement distances. A fundamental understanding remains elusive given the generic complexity of activated relaxation in supercooled liquids and the major complications of geometric confinement, interfacial effects and spatial inhomogeneity. We construct a predictive, quantitative, force-level theory of relaxation in free-standing films for the central question of the nature of the spatial mobility gradient. The key new idea is that vapor interfaces speed up barrier hopping in two distinct, but coupled, ways by reducing near surface local caging constraints and spatially long range collective elastic distortion. Effective vitrification temperatures, dynamic length scales, and mobile layer thicknesses naturally follow. Our results provide a unified basis for central observations of dynamic and pseudo-thermodynamic measurements.

Glass forming liquids undergo remarkable changes of dynamics at rather large confinement distances; in some cases shifts of the apparent vitrification temperature commence at 25-50 nm or beyond for polymer films¹⁻⁵. It has long been hoped this phenomenon holds critical clues about cooperative relaxation in bulk supercooled liquids⁶, but this remains unrealized due to the strong effect of interfaces, e.g., vapor vs. solid, surface chemistry². This problem is also crucial

for diverse materials applications⁷ and the formation of “ultra-stable” glasses⁸. A major mystery is the breakdown of accepted inter-relationships between different experimental probes (e.g., thermodynamic vs. dynamic) that hold in the bulk.^{1,2,9,10} However, it is widely acknowledged that the central question is the nature of a spatial gradient of mobility^{2,11-13}.

Time-dependent measurements are the most fundamental measure of glassy dynamics.

Recent experiments¹⁴ on *free-standing* polymer thin films find a 2-step decay of a probe molecule reorientational correlation function, $C(t)$, at ~ 10 - 30 K below the bulk glass transition temperature, T_g . This suggests a fast relaxing (by ~ 3 - 4 orders of magnitude) population of segments within several nm of the vapor interface corresponding to a temperature-dependent “mobile layer”^{14,15}, and a slow bulk-like population in the film interior. Not far above T_g the 2-step decay seems to disappear with the slow and fast processes “merging”. The generality of such phenomena is suggested by their near independence of polymer chemistry and chain length¹⁴, a ~ 7 decade speed up of diffusion¹⁶ at T_g and viscous flow¹⁷ of molecular glass-formers near the film surface, reduced interfacial viscosity¹⁸, and other measurements¹⁹. Especially notable is the nanoparticle embedding measurements which directly detect a mobile surface layer.¹⁵

Theoretical progress has been modest^{2,13,20,21} due to the inherent complexity of bulk activated relaxation, confinement and interfacial interactions. Simulations^{2,13,22,23} provide valuable insights but cannot access the deeply supercooled regime since they probe only down to of order the dynamic crossover temperature^{6,13}, T_c . Here, the bulk relaxation time is ~ 8 - 10 orders of magnitude faster than at T_g , the mobility enhancement at a free surface is only ~ 3 - 4 orders of magnitude, and a 2-step form of $C(t)$ is not observed^{2,13,23}. In this Communication we construct a no adjustable parameter, force-level theory of the mobility gradient, and determine its multi-variant consequences in free-standing^{2,3,24-26} films. The key idea is that vapor interfaces accelerate hopping by *both* reducing near surface local caging constraints and long range collective elastic distortion. Effective vitrification temperatures and length scales naturally follow.

The focus is on dynamics, but contact is made with pseudo-thermodynamic measurements¹⁻³.

The enabling foundation for our work is the bulk “elastically collective nonlinear Langevin equation” (ECNLE) theory^{27,28} based on the concept of a particle displacement, $r(t)$, dependent microscopic *dynamic* free energy, $F_{dyn}(r)$, that quantifies the effective force on a moving particle due to its surroundings (see Figure 1). For a fluid of spheres (diameter, d), $F_{dyn}(r) = F_0(r) + F_{cage}(r)$, where $F_0(r) = -3k_B T \ln(r)$ quantifies the driving force for unbounded diffusion, and $F_{cage}(r)$ quantifies intermolecular constraints which favor spatial localization and solid-like behavior and can be *a priori* calculated²⁸ from knowledge of fluid density ρ and the radial distribution function, $g(r)$, or structure factor. Key features of $F_{dyn}(r)$ include the barrier for *local* cage re-arrangement, ΔF_B , transient localization length, r_{loc} , barrier location, r_B , and jump distance, $\Delta r \equiv r_B - r_{loc} \approx 0.2 - 0.4d$. For deeply supercooled liquids, as originally proposed phenomenologically by Dyre²⁹, activated hopping requires a small expansion of the nearest neighbor shell and harmonic elastic distortion of the surrounding medium, resulting in an additional, spatially *non-local*, collective barrier^{27,28}:

$$\Delta F_{elastic}^{bulk} = \rho (K_0 / 2) \int_{r_{cage}}^{\infty} dr 4\pi r^2 u^2(r) \quad (1)$$

The displacement field²⁹ outside the cage radius ($r_{cage} \approx 1.5d$) is $u(r) = \Delta r_{eff} (r_{cage} / r)^2$, the cage dilation scale is $\Delta r_{eff} \propto \Delta r^2 / r_{cage} \leq r_{loc}$, and the spring constant describing localization (and dynamic shear modulus) is $K_0 = 3k_B T / r_{loc}^2$. The elastic barrier, $\Delta F_{elastic}^{bulk} \approx 12\phi \Delta r_{eff}^2 r_{cage}^3 d^{-3} K_0$, plays the central role in the deeply supercooled regime,

$\tau_\alpha > 10^{-7\pm 1}s$, and involves long range (scale invariant) motion with 90% of its total value requiring cooperative displacements out to a distance $\sim 13d$ from the cage center²⁸.

Bulk ECNLE theory is rendered quantitatively predictive for thermal liquids by mapping²⁸ molecules to an effective hard sphere fluid that exactly reproduces the equilibrium dimensionless density fluctuation amplitude or compressibility of the real system, $S_0(T) = \rho k_B T \kappa_T$. This yields a temperature and material-specific effective packing fraction, $\phi(T)$, which determines structure and dynamical constraints. The resultant theory accurately captures relaxation in van der Waals liquids (e.g., orthoterphenyl (OTP), trisnaphthylbenzene (TNB)) over 14 decades in time^{27,28}.

An interface can locally modify density, compressibility and molecular orientation. Our hypothesis for free-standing films (consistent with lack of measurable density changes) is these are second order effects and are ignored here. Rather, we emphasize three *generic* physical mechanisms of how a free surface modifies the spatially nonlocal activated relaxation event (Fig.1): (i) a “surface” effect close to the interface associated with reduced caging constraints, (ii) a long range “confinement” effect mainly due to collective elastic physics, and (iii) strong coupling between (i) and (ii) via a spatial gradient of elastic stiffness and cage expansion amplitude.

Cage rearrangement occurs via relatively large amplitude hopping (plot “a” in Fig.1) with a barrier due to forces exerted by nearest neighbors^{27,28}. Within a distance r_{cage} from a free surface, caging forces are reduced due to missing neighbors and hence $F_{cage}(r) \rightarrow \gamma(z)F_{cage}^{(bulk)}(r)$, where an elementary geometric calculation yields the ratio of nearest neighbors a distance z from the

surface relative to its bulk analog as: $\gamma(z) = 0.5 - 0.25(z/r_{cage})^3 [1 - 3(r_{cage}/z)^2]$ for $z \leq r_{cage}$. For $z > r_{cage}$, $\gamma \rightarrow 1$ and the bulk $F_{dyn}(r)$ is recovered; when $z \rightarrow 0$, $\gamma \rightarrow 0.5$, corresponding to missing half of the nearest neighbors at the surface²¹.

The elastic penalty associated with long range displacements is also weakened near the interface due to missing neighbors (plot “b” in Fig.1). This softening decreases continuously with distance from the surface, becoming bulk-like (plot “c”) deep in the film, as reflected in the color gradient darkening in Fig.1. Since there are no particles outside the film, the free surface effectively “cuts off” part of the collective barrier. We treat this effect as a simple cut off of the elastic deformation field thereby yielding :

$$\Delta F_{elastic}(z) = (\rho/2) \int_V d\vec{r} u(\vec{r}; z)^2 K_0(\vec{r}) \quad (2)$$

where V is the film volume. The strain field now depends on *both* the distance from the cage center and the location of the relaxation event in the film. The mean time associated with activated barrier crossing follows as²⁸

$$\frac{\tau_\alpha}{\tau_s} = 1 + \frac{2\pi(k_B T / d^2)}{\sqrt{K_0 K_B}} e^{(\Delta F_B + \Delta F_{elastic})/k_B T} \quad (3)$$

where K_0 , the barrier curvature K_B , both barriers, and the alpha time *all* depend on location in the film and its thickness, z and h , respectively; τ_s is the known, non-activated, bulk, short time relaxation process time scale²⁸. Calculation of the relaxation time function $\tau_\alpha(T, h, z)$ then allows the prediction of characteristic length scales and apparent vitrification temperatures relevant to diverse experiments.

We illustrate our central predictions using equilibrium $S_0(T)$ input³⁰ for polystyrene (PS) melts and the Kuhn length³¹ (l_K , twice the persistence length) as the dynamically relevant coarse graining variable. This corresponds to a liquid of disconnected Kuhn spheres, in the spirit of the molecular liquid mapping²⁸; for PS, $d=l_K \sim 1.2$ nm. All calculations are nearly identical for molecules such as OTP and TNB²⁸. Spatial gradients of dynamical properties are a continuous function of location in the film, but one should keep in mind that experiments have a finite resolution, e.g., $\sim(0.5-1)d$.

The main frame of Fig.2 shows the local cage, long range elastic, and total barriers, as a function of nondimensionalized film location $\zeta = 1 - 2z/h$, each normalized by its bulk value. Results are for $h=36$ nm $\sim 30d$ at the bulk T_g , defined as when $\tau_\alpha = 100s$; the bulk barriers are $\Delta F_B \approx 14k_B T$ and $\Delta F_{elastic} \approx 18k_B T$. The local barrier is strongly reduced close to the surface and saturates to its bulk value a distance r_{cage} into the film. In *qualitative* contrast, the elastic barrier, while strongly reduced near the surface, is suppressed far into the film as a unique consequence of the nonlocal^{28,29} nature of the alpha process *and* its coupling to near surface cage weakening.

The inset of Fig.2 shows the corresponding relaxation time gradient at five temperatures that straddle the bulk T_g . The alpha time is massively faster near the surface, and varies weakly with temperature. On the scale of d , relaxation near the surface at the bulk T_g speeds up by $\sim 6-8$ orders of magnitude, consistent with (near) surface diffusion in molecular systems¹⁶. The calculation at 426 K mimics the dynamic crossover temperature, $T_c \sim 1.2T_g$, where the collective barrier is of minor importance. This is

the regime probed in simulations, and the long tail into the film is largely absent since elastic distortion is very weak, and the gradient covers only ~ 3 orders of magnitude.

The calculations in Fig.2 allow a film-averaged relaxation function, $C(t) = \langle e^{-t/\tau_\alpha(z)} \rangle_z$, to be computed, as shown in Figure 3. In a temperature window modestly below T_g , and a time window germane to experiment¹⁴, $C(t)$ decays in two steps both of which are nonexponential solely due to the spatial mobility gradient. The fast, surface-related process has a rather low amplitude of $\sim 15\%$, while the slower bulk-like process has an amplitude $\sim 80\%$. The fast process is of a highly stretched (KWW) form, $\sim e^{-(t/\tau_{KWW})^{\beta_K}}$, where $\beta_K \approx 0.5 \rightarrow 0.27$ for $T=376 \rightarrow 346$ K. In contrast, the slow process exhibits a much larger and far less temperature-dependent $\beta_K \approx 0.9 \rightarrow 0.8$. The inset of Fig.3 shows the fast process time grows more slowly with cooling, becoming ~ 2 orders of magnitude shorter than the slow process. Far enough above the bulk T_g , a two-KWW fit is not sensible since the mobility gradient is much weaker (per in simulations^{13,22,23}) and the fast process falls outside the experimental time window¹⁴. We estimate via extrapolation a ‘‘merging’’ temperature at $\sim T_g + 25K$; experiments find $\sim T_g + 15K$.

The inset of Fig. 3 also shows a mobile liquid-like layer thickness, z^* , defined as the part of the film that relaxes faster than 100s. We find, e.g., $z^* \sim 2-3$ nm at 5K below the bulk T_g , and results for different film thicknesses essentially overlap except at T_g where (by definition) $z^* \rightarrow h/2$. A measureable mobile layer is predicted to be undetectable 30-40 K below T_g if the length scale resolution is $\leq d$. Other experiments with different resolutions^{15,19} report mobile layers 50-

80K below T_g , which is not inconsistent with our results in Fig.3.

All calculations in Figs. 2 and 3 are in qualitative accord with recent probe rotation measurements¹⁴. But there are quantitative deviations, e.g., the degree of stretching, and difference between the fast and slow relaxation times (2 vs. $\sim 3-4$ orders of magnitude), are smaller than observed. This is perhaps unsurprising given the theory and molecular model are approximate, experiments measure probe (not matrix) dynamics, the space-time resolution issue, and the existence of a relaxation time distribution in the bulk ignored here for simplicity.

We now consider the subtle question of an effective glass transition temperature^{1,2,32}. The main frame of Figure 4 shows a purely dynamical T_g defined as when the film averaged relaxation time reaches 100s, $\langle \tau_\alpha(z) \rangle_h |_{T_g} = 100s$ (corresponding, e.g., to a dielectric loss inverse peak frequency), and a “thermodynamic-like” alternative, $\langle T_g(z) \rangle_h$, where $\tau_\alpha(T_g(z;h)) \equiv 100s$; representative T_g -gradients are shown in the inset. The $\langle T_g(z) \rangle_h$ results show a significantly larger T_g drop than the purely dynamic analog as a consequence of how the mobility gradient is averaged. They are reminiscent of pseudo-thermodynamic measurements; e.g., at $h=10$ nm, $\langle T_g(z) \rangle_h$ decreases by $\sim 20K$, consistent with ellipsometry experiments for ~ 10 nm low and moderate molecular weight free-standing PS films^{3,24} that find a $\sim 25K$ T_g reduction. The thickness dependences are well fit (solid curves) by the empirical form that describes various experiments and simulations¹³, $T_g(h) = T_{g,bulk} (1 + \xi/h)^{-1}$, with $\xi < d$.

To make direct contact with ellipsometry data we construct a thermodynamic *effective* 2-layer model for the thermal expansivity per ref.³². Using the computed mobile layer thickness, z^* , one has $\alpha_{eff}(T) = \alpha_g(1 - 2z^*(T)/h) + \alpha_l 2z^*(T)/h$, where the liquid (glass) $\alpha_l = .0004K^{-1}$ ($\alpha_g = .0001K^{-1}$). Taking the film thickness at a low T_0 to be h_0 , one has $h(T)/h_0 = 1 + \int_{T_0}^T dT' \alpha_{eff}(T')$. Representative calculations (inset of Fig.4) show the key experimental features¹⁻³ are captured, including decreasing (increasing) contrast (breadth) of the *apparent* liquid \rightarrow glass transition as the film thins. The T_g values determined from the intersection of linear fits to the high and low temperature regimes are shown as open circles in the main frame of Fig. 4. Very interestingly, they agree essentially exactly with our $\langle T_g(z) \rangle_h$ calculations. These results provide new insights concerning the connection between an apparent T_g determined by falling out of thermodynamic equilibrium and one deduced based on equilibrated dynamics. The ideas³² that the ellipsometric T_g is “some kind of average of the gradient of τ_α ”, the kink in $h(T)$ does not indicate a real thermodynamic glass transition but rather reflects a mobile layer, and the dilatometric T_g is a convolution of enhanced surface mobility and a dynamical penetration length, all find theoretical support in our work.

In conclusion, we have constructed a quantitative, force level theory for how confinement in free-standing thin films introduces a mobility gradient as encoded in $\tau_\alpha(T, z, h)$. Diverse consequences appear consistent with experiment, and the theory has demonstrated^{27,28} material-specific predictive power. Of course,

much remains to be done, including incorporating anisotropic corrections to our simple cut off model of a radially symmetric elastic deformation field. Nonetheless, the present approach provides a foundation to treat diverse phenomena such as puzzling influences of chemistry on T_g shifts³³, explicit effects of polymer connectivity, the consequences of solid surfaces, mechanical properties³⁴, and non-planar geometries such as

spherical droplets³⁵. Work in all these directions is in progress.

Acknowledgement. This work was supported by the U.S. Department of Energy, Basic Energy Sciences, Materials Science Division via Oak Ridge National Laboratory. Informative discussions with Mark Ediger, Zahra Fakhraai and Greg McKenna are gratefully acknowledged.

References

- 1) M. Alcoutlabi and G.B. McKenna, *J. Phys.: Condens. Matt.* **17** R461-R524 (2005).
- 2) M. D. Ediger and J. A. Forrest, *Macromol.* **47**, 471-478 (2014).
- 3) J.A. Forrest and K. Dalnoki-Veress, *Adv. Coll. Interf. Sci.* **94**, 167-196 (2001).
- 4) R. Richert, *Ann. Rev. Phys.* **62**, 65-84 (2011).
- 5) C.L. Jackson and G.B. McKenna, *J. Non-Cryst. Sol.* **131-133**, 221-224 (1991); J.L. Keddie, R.A.L. Jones and R.A. Cory, *Europhys. Lett.* **27**, 59-64 (1994).
- 6) M.D. Ediger and P. Harrowell, *J.Chem.Phys.* **137**, 080901 (2012); L.Berthier and G.Biroli, *Rev.Mod.Phys.*, **83**, 587 (2011).
- 7) A. Bansal, H.C. Yang, C.Z. Li, K.W. Cho, B.C. Benicewicz, S.K. Kumar and L.S. Schadler, *Nat. Mat.*, **4**, 693 (2005); J. Berriot, H. Montes, F. Lequeux, D. Long and P. Sotta, *Macromol.* **35**, 9756 (2002); J.Moll and S.K.Kumar, *Macromol.*, **45**, 1131 (2012); P. Rittigstein, R.D. Prestley, L.J. Broadbelt and J.M. Torkelson, *Nat. Mat.*, **6**, 278 (2007).
- 8) K.L. Kearns, S.F.Swallen, M.D. Ediger, T.Wu, Y.Sun and L.Yu, *J.Phys.Chem.B* **112**, 4934 (2009).
- 9) M. Tress, M. Erber, E.U. Mapese, H. Huth, J. Mueller, A. Serghei, C. Schick, K.J. Eichorn, B. Volt and F. Kremer, *Macromol.* **43**, 9937 (2010); V.M. Boucher, D. Cangialosi, H. Yin, A. Schönhals, A. Alegría and J. Colmenero, *Soft Matter* **8**, 5119-5122 (2012).
- 10) K. Fukao and Y. Miyamoto, *Phys. Rev. E* **64**, 011803 (2001); S. Kawana and R.A.L. Jones, *Phys. Rev. E* **63**, 021501 (2001).
- 11) P.G. de Gennes, *Eur. Phys. J. E* **2**, 201-205 (2000).
- 12) C.J. Ellison and J.M. Torkelson, *Nat. Mat.* **2**, 695-700 (2003).
- 13) J. Baschnagel and F. Varnik, *J. Phys: Condens. Matt.* **17**, R851-R953 (2005).
- 14) K. Paeng, S.F. Swallen and M.D. Ediger, *J. Am. Chem. Soc.* **133**, 8444-8447 (2011); K. Paeng and M.D. Ediger, *Macromol.*, **44**, 7034 (2011); K. Paeng, Richert, R. and M.D. Ediger, *Soft Matter* **8**, 819-826 (2012).

- 15) D. Qi, M. Ilton, and J. Forrest, *Eur. Phys. J. E* **34**, 1-7 (2011).
- 16) L. Zhu, C.W. Brian, S.F. Swallen, P.T. Straus, M.D. Ediger and L. Yu, *Phys. Rev. Lett.* **106**, 256103 (2011).
- 17) C.R. Daley, Z. Fakhraai, M.D. Ediger and J.A. Forrest, *Soft Matter* **8**, 2206 (2012).
- 18) Y. Chai, T. Salez, J.D. McGraw, M. Benzaquen, K. Dalnoki-Veress, E. Raphael and J.A. Forrest, *Science*, **343**, 994 (2014); Z. Yang., Y. Fujui, F.K. Lee, C.-H. Lam and O.K.C. Tsui, *Science*, **328**, 1676 (2010).
- 19) Z. Fakhraai and J.A. Forrest, *Science* **319**, 600-604 (2008).
- 20) J.E.G. Lipson and S. T. Milner, *Macromol.* **43**, 9874-9880 (2010); S. T. Milner and J.E.G. Lipson, *Macromol.* **43**, 9865-9873 (2010).
- 21) J.D. Stevenson and P.G. Wolynes, *J. Chem. Phys.* **129**, 234514 (2008).
- 22) J.A. Torres, P.F. Nealey and J.J. de Pablo, *Phys. Rev. Lett.* **85**, 3221-3224 (2000).
- 23) A. Shavit and R.A. Riggleman, *Macromol.* **46**, 5044-5052 (2014).
- 24) J.A. Forrest, K. Dalnoki-Veress, J.R. Stevens and J.R. Dutcher, *Phys. Rev. Lett.* **77**, 2002-2005 (1996).
- 25) J. Mattsson, J.A. Forrest and L. Börjesson, *Phys. Rev. E* **62**, 5187-5200 (2000).
- 26) J.E. Pye and C.B. Roth, *Phys. Rev. Lett.* **107**, 235701 (2011).
- 27) S. Mirigian and K.S. Schweizer, *J.Phys.Chem.Lett.*, **4**, 3648 (2013).
- 28) S. Mirigian and K.S. Schweizer, *J.Chem.Phys.*, **140**, 194506 (2014); S. Mirigian and K.S. Schweizer, *J.Chem.Phys.*, **140**, 194507 (2014).
- 29) J.C. Dyre *J.Non-Cryst.Solids* **235**, 142 (1998); J.C. Dyre *Rev. Mod. Phys.* **78**, 953(2006).
- 30) The effective hard sphere packing fraction is²⁸

$$\phi(T; A, B, N_s) = 1 + \sqrt{S_0^{\text{expt}}(T)} - \sqrt{S_0^{\text{expt}}(T) + 3\sqrt{S_0^{\text{expt}}(T)}}$$
where $S_0^{\text{expt}} = N_s^{-1}(-A + B/T)^{-2}$, $A=0.6$ and $B=1083$ K for polystyrene [K.S.Schweizer and E.J.Saltzman, *J. Chem. Phys.*, **121**, 1984 (2004)], and $N_s = 38$ based on the Kuhn length mapping.
- 31) T.Inoue and K.Osaki, *Macromol.* **29**, 1595 (1996); T.P.Lodge and T.C.B.McLeish, *Macromol.*, **33**, 5278 (2000).
- 32) J.A. Forrest and K. Dalnoki-Veress, *ACS Macro. Lett.* **3**, 310-314 (2014); J.A. Forrest, *J. Chem. Phys.* **139**, 084702 (2013).
- 33) C.J. Ellison, M.K. Mindra and J.M. Torkelson, *Macromol.*, **38**, 1767 (2005).
- 34) P.A.O'Connell, J.Wang, T.A.Ishola and G.B.McKenna, *Macromol.*, **45**, 2453 (2012).
- 35) C. Zhang, Y. Guo, and R.D. Priestley, *Macromol.* **44**, 4001-4006 (2011).

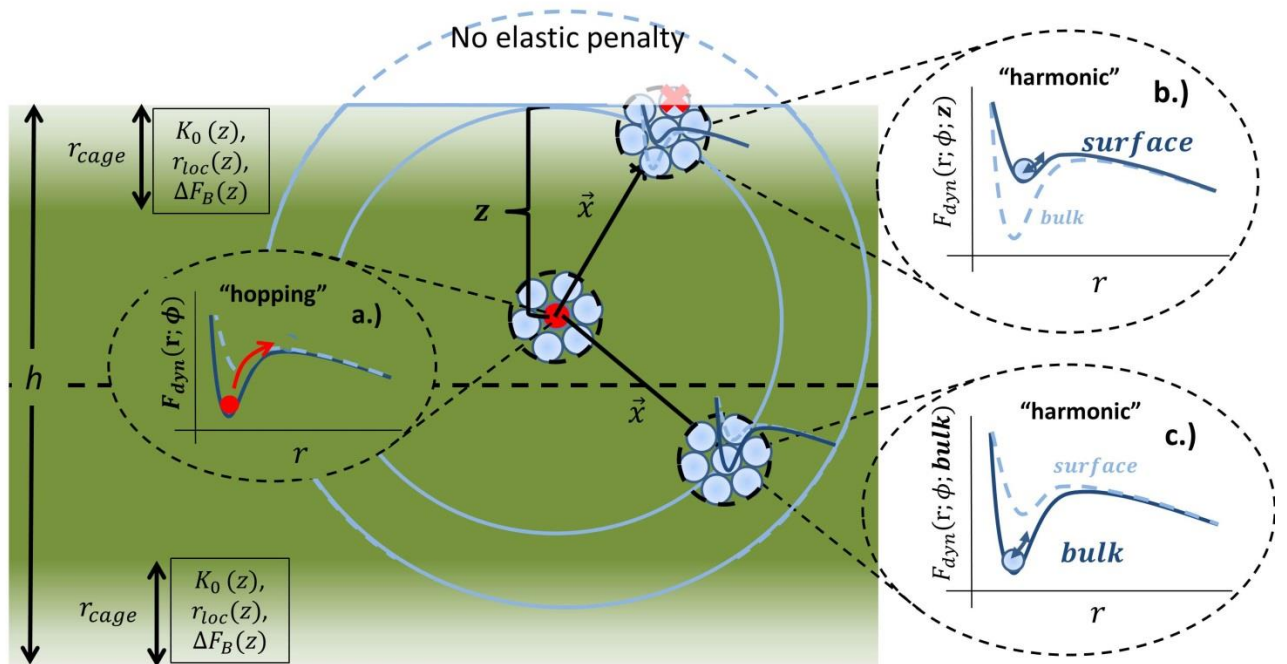


Fig. 1. Conceptual schematic of dynamical processes and key dynamic free energy features. The film thickness is h and the distance of a local rearrangement event from the film surface is z . a.) Hopping requires surmounting a local barrier. b.) Particles near the surface experience a reduced caging force due to missing neighbors, resulting in a film-location-dependent softer confinement potential. c.) Particles far from a free surface experience the bulk dynamic free energy. The long range elastic barrier is a sum of the elastic energy penalty for harmonic motion throughout the spatially heterogeneous film.

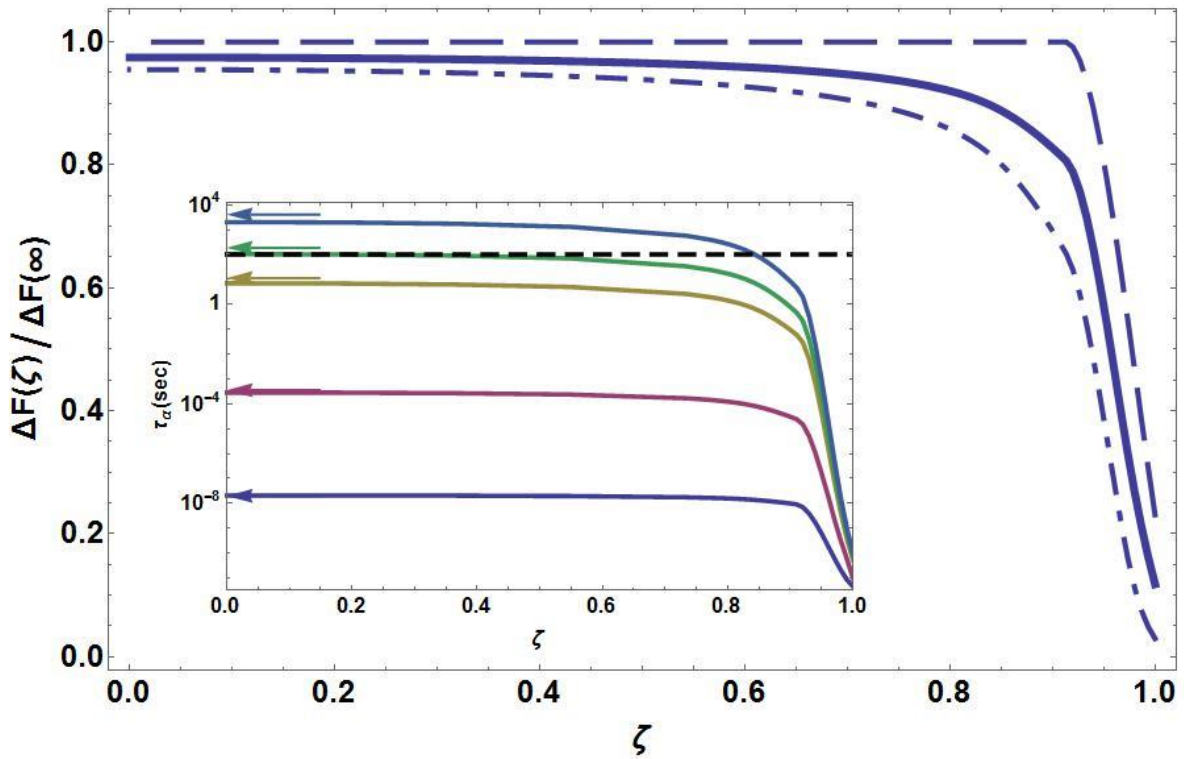


Fig 2. Local cage (dashed), elastic (dash-dot), and total (solid) barriers for a film thickness $h=36$ nm at the bulk T_g as a function of reduced location, $\zeta = 1 - 2z/h$; each barrier is normalized by its bulk value. Inset: Corresponding relaxation time profiles at 426K (blue, near the bulk T_c), 386K (red), 361K (yellow), 356K (green, predicted bulk T_g), and 351K (gray). The horizontal black dashed line indicates kinetic vitrification, and arrows along the vertical axis indicate the bulk alpha time.

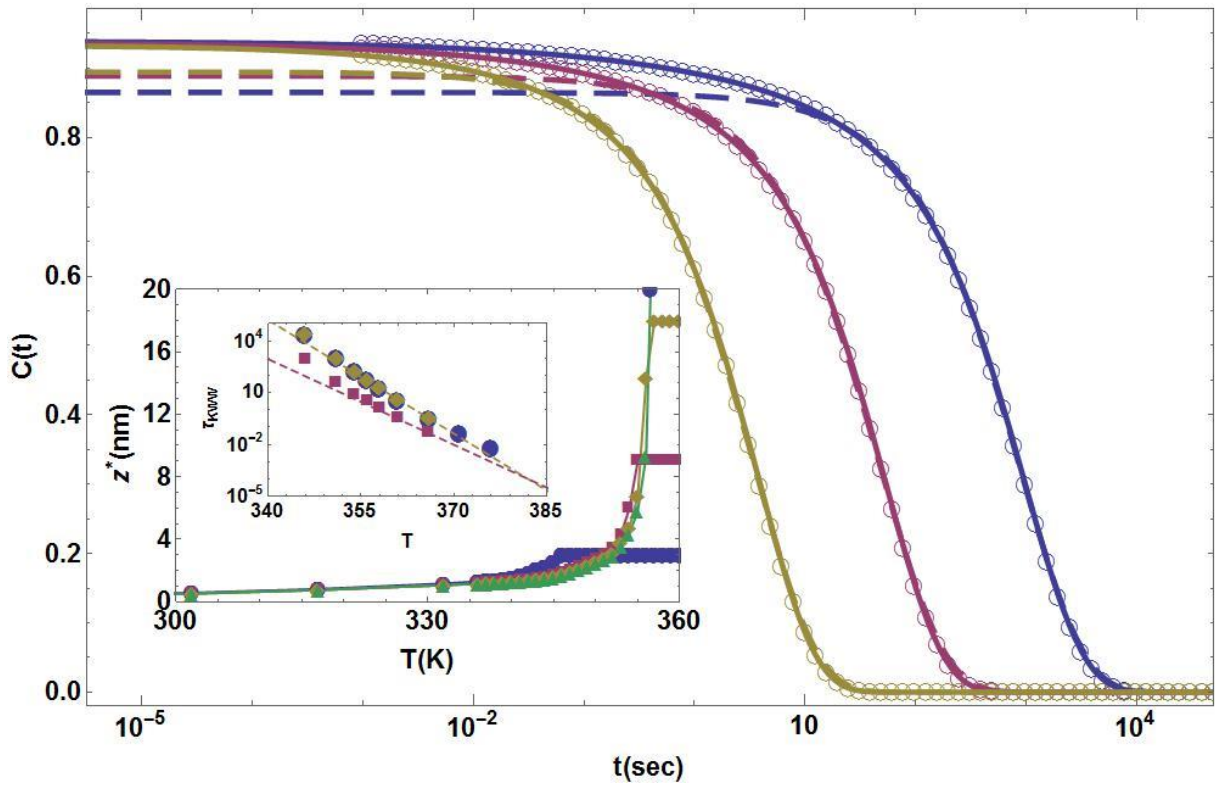


Fig. 3. Relaxation function for $h=36$ nm at $T = 351$ K (blue circles), 356 K (red circles, bulk T_g) and 361 K (yellow circles). The solid (dashed) curves are double (single) KWW fits. Insets: Corresponding extracted relaxation times with an apparent merging point determined via extrapolation. Mobile layer thickness (z^* in nm) as a function of temperature for 6 nm (blue), 18 nm (red), 36 nm (yellow) and 180 nm (green) films.

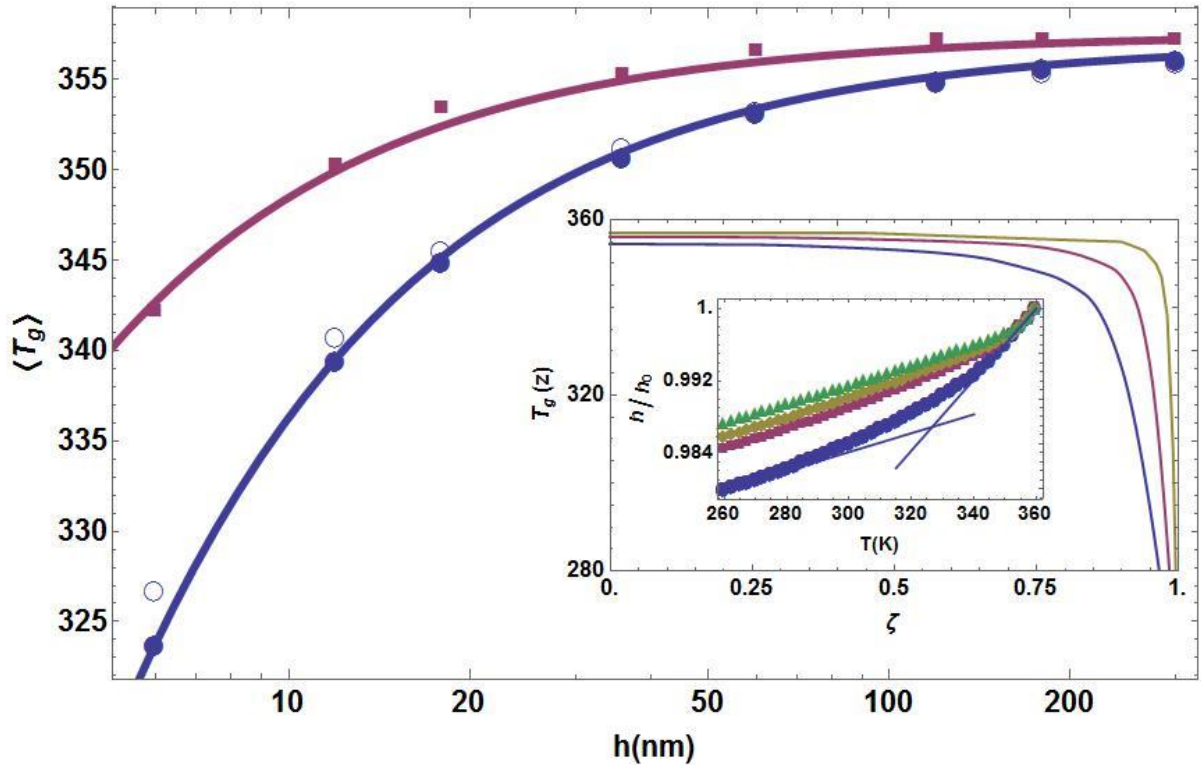


Fig 4. Film-averaged glass transition temperatures as a function of thickness: $\langle T_g(z) \rangle_h$ using the vitrification profile of the inset (closed circles), T_g based on the dynamic criterion $\langle \tau_\alpha(z) \rangle_h |_{T_g} = 100\text{s}$ (red squares), and thermodynamic ellipsometric result (open circles) based on the $h(T)$ calculations of the inset. Insets: Kinetic T_g profile for film thicknesses of 18nm (blue), 36nm (red) and 120nm (yellow). Temperature variation of the film thickness for the same systems in the inset of Fig.3: 6nm (blue), 18nm (red), 36nm (yellow) and 180nm (green) films; extraction of a T_g as measured using ellipsometry is indicated.